



# Efficient Quantum Circuit Compilation for Near-Term Quantum Advantage

Yuchen Guo <sup>1</sup> and Shuo Yang <sup>1,2,3,\*</sup>

<sup>1</sup>State Key Laboratory of Low Dimensional Quantum Physics and Department of Physics, Tsinghua University, Beijing 100084, China

<sup>2</sup>Frontier Science Center for Quantum Information, Beijing 100084, China

<sup>3</sup>Hefei National Laboratory, Hefei 230088, China

Quantum noise in real-world devices poses a significant challenge in achieving practical quantum advantage, since accurately compiled and executed circuits are typically deep and highly susceptible to decoherence. To facilitate the implementation of complex quantum algorithms on noisy hardware, we propose an approximate method for compiling target quantum circuits into brick-wall layouts. This new circuit design consists of two-qubit CNOT gates that can be directly implemented on real quantum computers, in conjunction with optimized one-qubit gates, to approximate the essential dynamics of the original circuit while significantly reducing its depth. Our approach is evaluated through numerical simulations of time-evolution circuits for the critical Ising model, quantum Fourier transformation, and Haar-random quantum circuits, as well as experiments on IBM quantum platforms. By accounting for compilation error and circuit noise, we demonstrate that time evolution and quantum Fourier transformation circuits achieve high compression rates, while random quantum circuits are less compressible. The degree of compression is related to the rate of entanglement accumulation in the target circuit. In particular, experiments on IBM platforms achieve a compression rate of 12.5 for  $N = 12$ , significantly extending the application of current quantum devices. Furthermore, large-scale numerical simulations for system sizes up to  $N = 30$  reveal that the optimal depth  $d_{\max}$  to achieve maximal overall fidelity is independent of system size  $N$ , suggesting the scalability of our method for large quantum devices in terms of quantum resources.

## INTRODUCTION

Achieving a quantum advantage involves a delicate competition between entanglement and decoherence. Recent experiments demonstrate the potential quantum advantage in random circuit sampling [1–3], where noisy intermediate-scale quantum (NISQ) devices [4] can generate highly entangled quantum states before they are destroyed by noise. Meanwhile, classical simulation using tensor network methods [5, 6] consumes significant computing resources [7, 8]. However, realizing the practical quantum advantage and solving valuable problems in physics or other fields beyond the capabilities of classical computers remains a much more challenging task [9]. The level of difficulty varies in different contexts. For instance, conventional quantum algorithms with theoretical promise, such as Shor’s factoring or Grover’s searching algorithms [10], require fault-tolerant quantum computers due to their reliance on non-local gates. On the other hand, heuristic quantum-classical hybrid algorithms, such as the variational quantum eigensolver [11, 12], face scalability challenges due to barren plateaus, which lead to exponentially increasing measurement costs when training parameterized quantum circuits [13, 14].

A recent experiment demonstrated quantum utility in simulating the time evolution of the Ising model using a discrete Trotter step of  $\tau = \pi/2$ , where the corresponding two-qubit gate can be directly compiled into a single CNOT gate along with other single-qubit gates [15]. However, accurately simulating time evolution—a key aspect in quantum many-body physics—typically involves much smaller Trotter steps. These smaller steps result in deeper quantum circuits that are more vulnerable to decoherence [16]. This creates a trade-off between the compilation errors introduced by the discrete Trot-

ter step and the circuit errors caused by noise. From another perspective, the accumulation of quantum entanglement in a Trotter circuit with small  $\tau$  progresses more slowly than in random quantum circuits, meaning that the entangling gates are not being fully utilized.

Fortunately, recent research [17–19] has shown that shallow quantum circuits can be used to approximate target quantum states or unitaries using various classical optimization techniques. However, the optimized circuits in these studies still involve arbitrary two-qubit gates that are not directly implementable on quantum hardware. In standard compilation strategies for superconducting quantum computers, a two-qubit gate is decomposed into three CNOT gates [20]. This increases both the classical optimization to train two-qubit gates and quantum compilation costs, making this process more resource-intensive. Moreover, these studies do not account for circuit noise, a significant constraint on the performance of state-of-the-art quantum devices.

In this paper, we propose a new approach to address these challenges by approximately compiling target quantum circuits while maximizing the overall fidelity, considering both compilation errors and noise effects. Our key innovation is the direct optimization of a brick-wall circuit composed of trainable single-qubit gates and fixed two-qubit CNOT gates. This eliminates the need for further compilation, allowing us to design a circuit that approximates the target quantum dynamics with high fidelity while maintaining shallow depth, making it suitable for accurate execution on a quantum computer. Numerical simulations demonstrate that our method consistently outperforms the original circuit regarding overall fidelity in many cases, with reduced circuit noise compensating for approximation errors. This is particularly evident in the time evolution of the critical Ising model and the quantum Fourier transformation (QFT) circuit, where the entanglement accu-

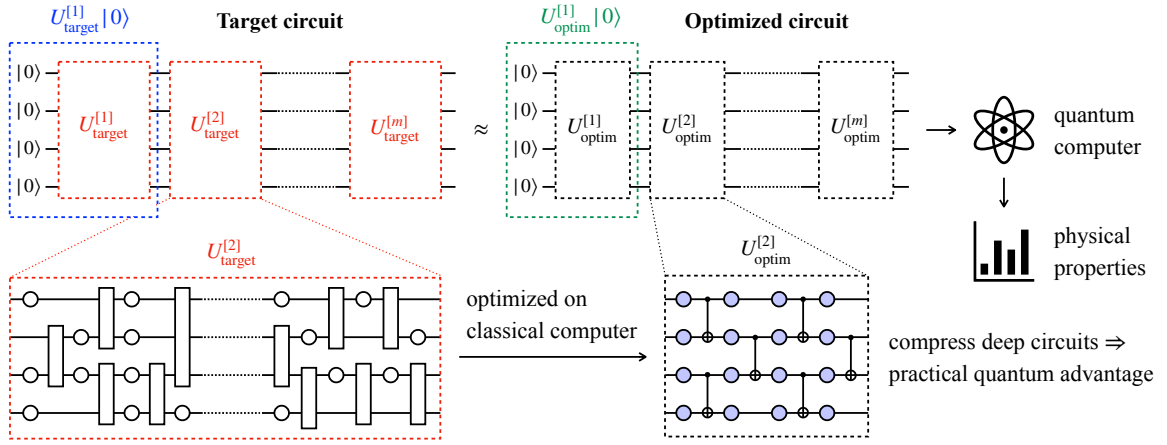


FIG. 1. The overall framework of this study. A deep quantum circuit is divided into several parts, each with shallow depth enabling classical simulation. Each part is replaced by a brick-wall circuit composed of trainable single-qubit gates and fixed CNOT gates. The optimized circuit is subsequently executed on a quantum computer, where relevant observables are measured and collected.

ulates slowly at each step. However, we observe little improvement for random circuits, which aligns with our intuitive expectations. Experiments on IBM quantum computers demonstrate the effectiveness of our method in compiling quantum circuits, as exemplified by the time evolution of the critical Ising model with  $N = 12$  qubits, a time interval  $\tau = 0.1$ , and 200 time steps compiled to an optimized circuit with depth  $d_{\text{optim}} = 48$ . Our approach is scalable to the number of qubits, paving the way for realizing a practical quantum advantage in near-term quantum devices before fault-tolerant quantum computing becomes feasible.

## RESULTS

### Approximate compilation of deep circuits

Our method for compiling a target quantum circuit  $U_{\text{target}}$  involves the following key steps, as outlined in Fig. 1.

1. Break down the target circuit into manageable parts.
2. Use a classical optimization algorithm to find an approximate compilation for each part.
3. Execute the optimized circuit on the quantum computer and measure relevant observables.

Our compilation algorithm cannot be applied directly to a deep circuit that offers a potential quantum advantage, as it cannot be classically simulated and optimized. Consequently, we assume the entire circuit consists of  $m$  parts as

$$U_{\text{target}} = U_{\text{target}}^{[m]} \circ U_{\text{target}}^{[m-1]} \circ \dots \circ U_{\text{target}}^{[1]}, \quad (1)$$

where each part  $U_{\text{target}}^{[j]}$  has a fixed depth  $d_{\text{target}}^{[j]}$  enabling a classical representation as a matrix product operator (MPO).

The second step is to optimize a reduced-depth quantum circuit for each part  $U_{\text{target}}^{[j]}$ . We assume that this optimized circuit has a brick-wall structure with trainable single-qubit gates and fixed CNOT two-qubit gates, as shown in Fig. 1. This structure can be directly executed on superconducting quantum computers without incurring additional costs. Moreover, there is a minor adjustment for handling the first part  $U_{\text{target}}^{[1]}$ , given that the input state  $|\psi_0\rangle$  of the quantum circuit is known in advance. Typically, this is set as a product state  $|0 \dots 0\rangle$ . Otherwise, the preparing circuit for the initial state can be incorporated into the computational circuit. For the problem we focus on, namely executing the compiled quantum circuits and obtaining measurement outcomes crucial for practical applications, the first part only needs to satisfy

$$U_{\text{optim}}^{[1]} |\psi_0\rangle \approx U_{\text{target}}^{[1]} |\psi_0\rangle. \quad (2)$$

For the remaining parts, we have

$$U_{\text{optim}}^{[j]} \approx U_{\text{target}}^{[j]}, \quad j = 2, \dots, m \quad (3)$$

Specifically, each part of the target circuit is simulated by a matrix product state (MPS) or MPO for  $U_{\text{target}}^{[1]} |\psi_0\rangle$  or  $U_{\text{target}}^{[j]} (j = 2, \dots, m)$ , respectively, with the standard truncation method and a large enough bond dimension  $D_{\text{target}}$  to guarantee the accuracy. This simulation is plausible if we fix the maximum depth of each part as a constant  $d_{\text{target}}^{[j]}$  independent of the system size  $N$ . The loss function is defined as follows

$$\Theta^{[1]} = \left\| U_{\text{optim}}^{[1]} |\psi_0\rangle - U_{\text{target}}^{[1]} |\psi_0\rangle \right\|_F^2, \quad (4)$$

$$\Theta^{[j]} = \left\| U_{\text{optim}}^{[j]} - U_{\text{target}}^{[j]} \right\|_F^2, \quad j = 2, \dots, m, \quad (5)$$

where  $\|\cdot\|_F$  denotes the Frobenius norm of an operator. We optimize single-qubit gates using the Riemannian optimization technique to ensure the preservation of the unitary condition [17, 19, 21, 22], combined with state-of-the-art automatic

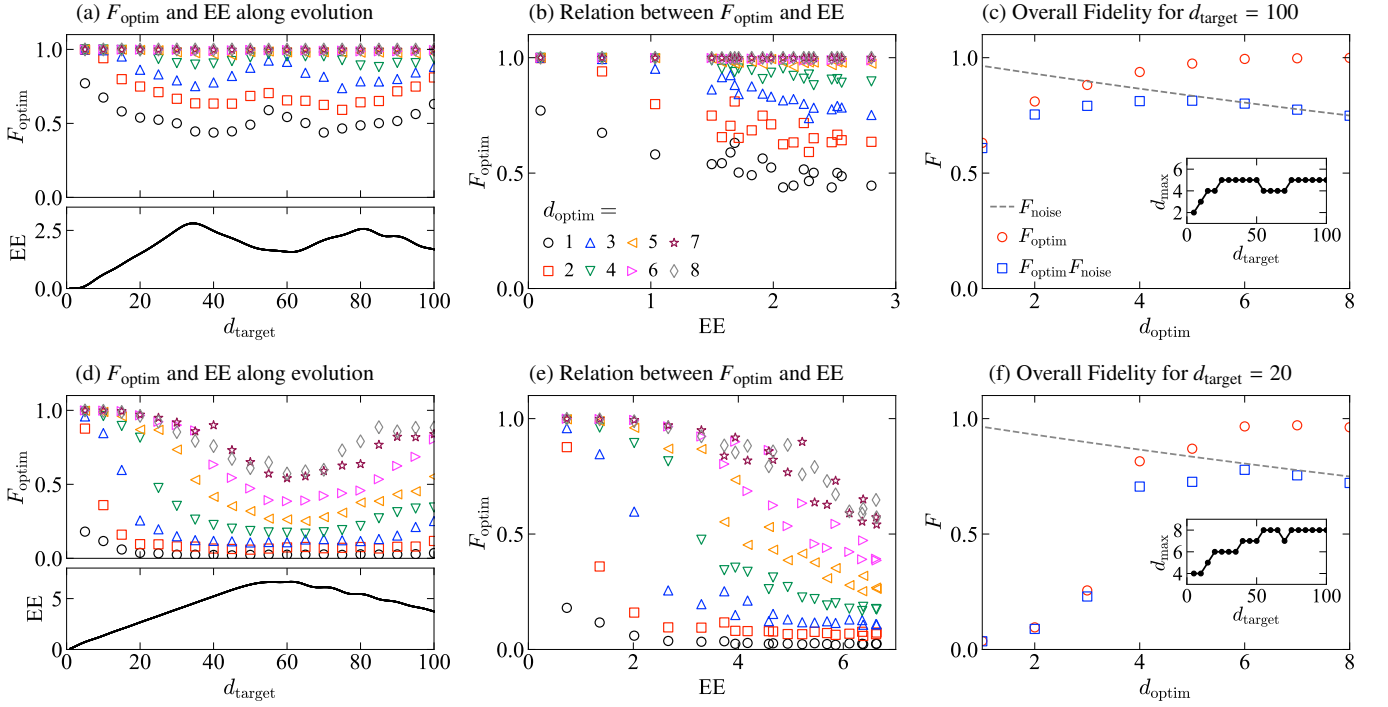


FIG. 2. Performance of circuit compilation for the time evolution of critical Ising model with  $N = 10$  and  $\tau = 0.1$ , simulated with  $D_{\text{target}} = 128$ . (a-c) Results for the output state from an initial product state. (d-f) Results for the entire unitary. (a, d) Optimization fidelity  $F_{\text{optim}}$  for different  $d_{\text{optim}}$  and EE along the evolution. (b, e) Relation between  $F_{\text{optim}}$  and EE for different  $d_{\text{optim}}$ . (c, f) Overall fidelity  $F_{\text{all}}$  for the state with  $d_{\text{target}} = 100$  and unitary with  $d_{\text{target}} = 20$ . Insets show the optimal depth  $d_{\text{max}}$  along the evolution. Note that (a), (b), (d), and (e) share a common legend plotted in (b).

differentiation [23, 24] and the Adam optimizer [25–27] (See Methods). In the following sections, the compression rate is defined as

$$\gamma^{[j]} = \frac{n_{\text{CNOT to compile } U_{\text{target}}^{[j]}}}{n_{\text{CNOT in } U_{\text{optim}}^{[j]}}}, \quad (6)$$

which evaluates the performance of our approximate compilation method compared to the standard one, focusing on the reduction of experimental cost and circuit noise. For a target circuit that also has a brick-wall circuit but with general two-qubit gates (such as time evolution of nearest-neighbor quantum models or commonly studied random circuits), the above expression simplifies to

$$\gamma^{[j]} = \frac{3d_{\text{target}}}{d_{\text{optim}}}, \quad (7)$$

where we utilize the fact that any two-qubit gate can be compiled by three CNOT gates.

### Numerical results for critical Ising model

In this section, we present numerical results for the time evolution  $e^{-iHt}$  of the critical Ising model with  $N = 10$ , whose

Hamiltonian is given by

$$H = - \sum_i \sigma_i^z \sigma_{i+1}^z - \sum_i \sigma_i^x. \quad (8)$$

We choose the first-order Trotter circuit with a time step  $\tau = 0.1$  and total evolution time  $t = 10$  as the target circuit  $U_{\text{target}} = (e^{-iH\tau})^{d_{\text{target}}}$  with  $d_{\text{target}} = 100$ . The target circuit with or without an initial product state is simulated using MPS or MPO with  $D_{\text{target}} = 128$ . After that, an optimized circuit is used to approximate the target circuit, with optimization fidelity  $F_{\text{optim}}$  shown in Fig. 2(a) and 2(d), respectively. Furthermore, we display the entanglement entropy (EE) of the quantum state or operator during time evolution, with the logarithm taken to the base 2.

Overall, the optimization fidelity is relatively higher when the initial state is fixed, which is as expected since the Hilbert space to be explored is much smaller in this case (about the square root of the entire unitary). From the perspective of quantum entanglement, the accumulation of EE is faster in the full unitary than in the time-evolving state (comparing the lower panels of Fig. 2(a) and 2(d)). In both cases, the entanglement capacity of the CNOT gate is bounded by a constant value of 1 for both state EE and operator EE. Specifically, preparing a thermalized quantum state with  $N$  qubits requires at least  $N/2$  layers of CNOT gates, aligned with the observation in Fig. 2(a) that  $d_{\text{optim}} = 5$  is sufficient for any target

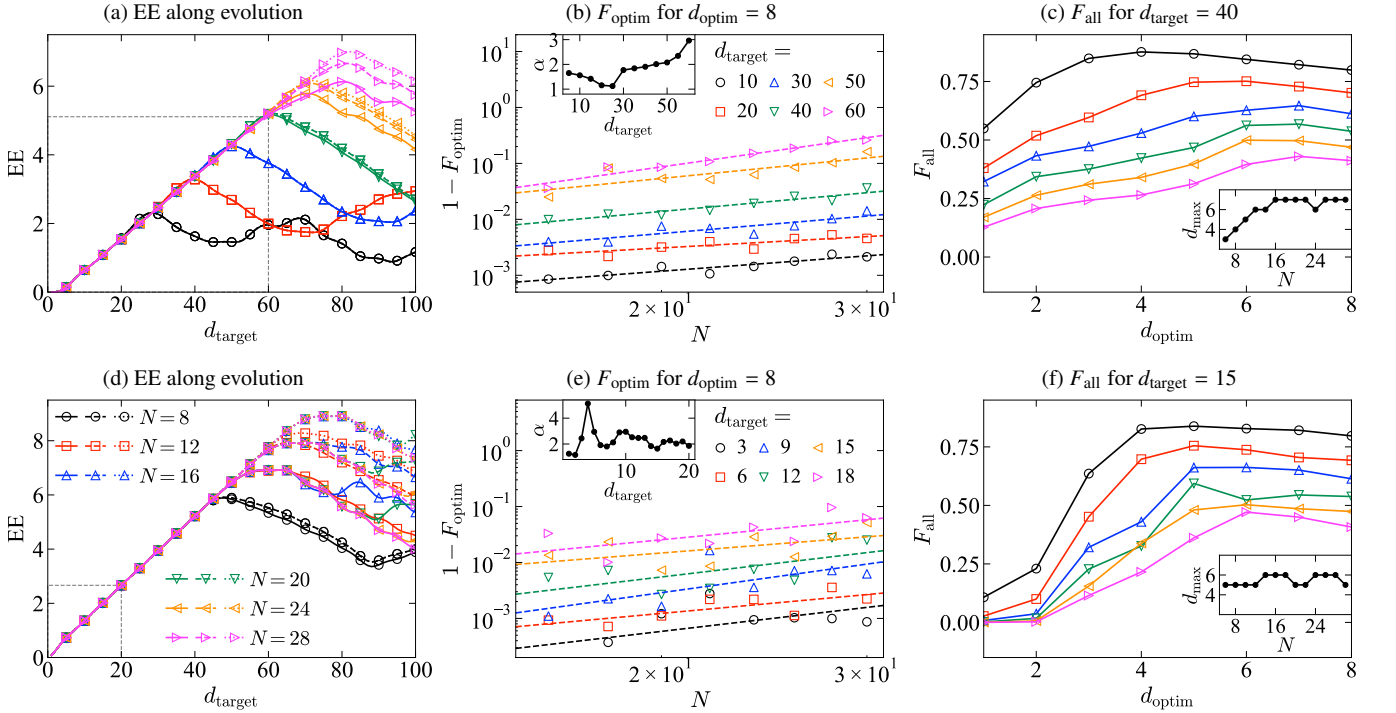


FIG. 3. The scalability of circuit compilation for the time evolution of critical Ising model with  $\tau = 0.1$ . (a-c) Results for the output state from an initial product state. (d-f) Results for the entire unitary. (a, d) EE dynamics for different  $D_{\text{target}}$  and  $N$  (solid lines for  $D_{\text{target}} = 128$ , dashed lines for  $D_{\text{target}} = 256$ , and dotted lines for  $D_{\text{target}} = 512$ ). Grey dashed frames mark the regimes suitable for efficient classical simulation and optimization. (b, e) Compilation error against increasing  $N$  on a log-log scale for different  $d_{\text{target}}$  and  $D_{\text{target}} = 128$ . Insets show the fitted exponent  $\alpha$  for  $1 - F_{\text{optim}} \sim N^\alpha$ . (c, f) Overall fidelity with varying  $d_{\text{optim}}$  for different  $N$  and  $D_{\text{target}} = 128$ . Insets show the optimal depth  $d_{\text{max}}$ . Note that (a), (c), (d), and (f) share a common legend plotted in (d).

circuit depth  $d_{\text{target}}$ . However, to approximate a unitary for long-time evolution, at least twice the depth (i.e.,  $N$  layers of CNOT gates) is necessary. Therefore, a higher compression rate can be achieved for the first part of the circuit than for the rest, i.e.,  $\gamma^{[1]} > \gamma^{[j]}$  for  $j = 2, \dots, m$ .

The above discussion implies a strong relation between  $F_{\text{optim}}$  and EE for a given  $d_{\text{optim}}$ , which is explicitly shown in Fig. 2(b) and 2(e) for the approximation of state and unitary, respectively. In other words, whether our approximate compilation method can effectively realize depth compression is determined by the rate of entanglement accumulation. Consequently, we expect the compression rate to strongly depend on the Trotter step with  $\gamma \sim 1/\tau$ . Notably, this result leads to the intriguing conclusion that only a constant depth is required to simulate time evolution with varying Trotter steps. This comes from the fact that EE converges to a constant value when  $t$  is fixed and  $\tau$  decreases. In this sense, simulating the target circuit using MPO simulation introduces only a classical overhead of  $t/\tau$ , while the quantum resource cost remains constant. However, it does not imply that arbitrary precision can be achieved, as compilation errors and noise effects (discussed below) limit the attainable accuracy. In contrast, for random quantum circuits exhibiting a ballistic entanglement membrane [28], any approximation in the compilation introduces a non-negligible error, as demonstrated later, hindering

the application of our scheme.

Nevertheless, real quantum devices in the NISQ era are affected by noise, requiring a comprehensive consideration of various error sources. To estimate the overall fidelity, we define  $F_{\text{all}} \equiv F_{\text{optim}}F_{\text{noise}}$ , where  $F_{\text{noise}}$  accounts for the noise effects on the final performance. We model this term as  $F_{\text{noise}} = (1 - \epsilon^{[2]})^{n_{\text{CNOT}}}$ , with  $\epsilon^{[2]} = 4 \times 10^{-3}$  representing the error rate for a two-qubit CNOT gate, based on the latest advances in superconducting quantum computers [29]. Here,  $n_{\text{CNOT}} = (N - 1)d_{\text{optim}}$  is the number of CNOT gates in the optimized brick-wall circuit. The curves in Fig. 2(c) and 2(f), corresponding to the state with  $d_{\text{target}} = 100$  and unitary with  $d_{\text{target}} = 20$ , respectively, show a competition between the compilation error and noise effects. The insets present optimal depths  $d_{\text{max}}$  that maximize the overall fidelity throughout the evolution, following a trend similar to the corresponding EE dynamics of the target circuit.

### Scalability to larger systems

In this section, we explore the scalability of our scheme with respect to system size. We begin by simulating the EE dynamics in Fig. 3(a) and 3(d) for systems up to  $N = 30$  qubits, with varying bond dimensions (solid lines for  $D_{\text{target}} =$

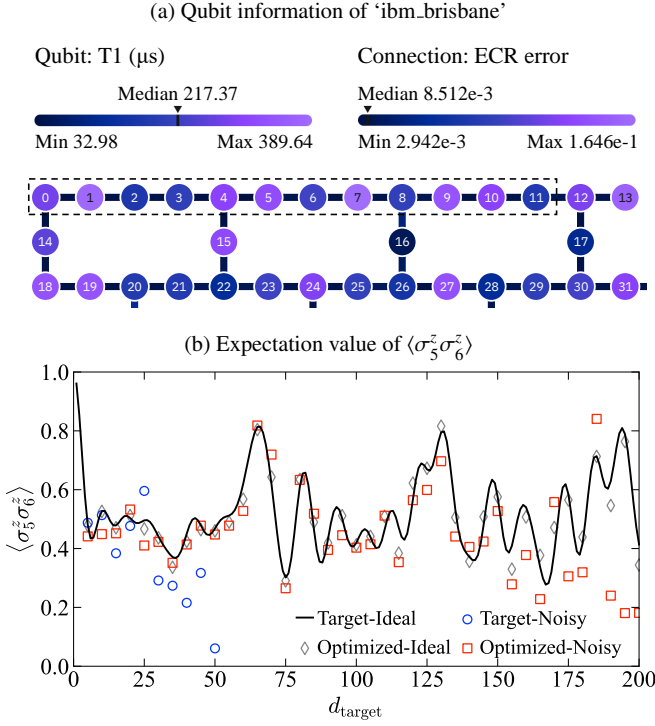


FIG. 4. Real experiments on IBM quantum hardware. (a) Hardware information for 'ibm\_brisbane'. Qubits 0 ~ 11 are used in our experiments. (b) Expectation values of  $\sigma_5^z \sigma_6^z$  compared for ideal and noisy, target and optimized circuits.

128, dashed lines for  $D_{\text{target}} = 256$ , and dotted lines for  $D_{\text{target}} = 512$ ). The convergence of EE as the bond dimension  $D_{\text{target}}$  increases confirms that the simulation of the target circuit is accurate, which is essential for the subsequent circuit compilation process. Correspondingly, to ensure that each part of the circuit remains shallow and implementable by classical simulation and optimization, we bound the target circuit depths by constants  $d_{\text{optim}}^{[1]} = 60$  and  $d_{\text{optim}}^{[j]} = 40$  for  $j = 2, \dots, m$ , independent of system size. Meanwhile, the results in Fig. 2(d) suggest that compiling a unitary with  $d_{\text{target}} = 20$  unitary to an optimized depth of  $d_{\text{optim}} = 8$  yields satisfactory performance (with  $F_{\text{optim}} = 0.963$ ). Thus, we limit our analysis to shallow circuits with depths smaller than  $d_{\text{optim}}^{[j]} = 20$  for  $j = 2, \dots, m$  while still achieving a large compression rate of  $\gamma = 7.5$  that significantly reduces the noise effects typically associated with deeper circuits.

The final accuracy of our scheme is determined by the compilation fidelity of each part, especially the scaling law with a given constant depth but increasing  $N$ . Specifically, we compare the trend of  $1 - F_{\text{optim}}$  with increasing  $N$  for a fixed optimized circuit depth  $d_{\text{optim}} = 8$  and different target circuit depths up to  $d_{\text{target}} = 60$  for the state in Fig. 3(b) and up to  $d_{\text{target}} = 20$  for the unitary in Fig. 3(e), respectively, on a log-log scale. The linearly fitted slopes in the insets reveal a power law of  $1 - F_{\text{optim}} \sim N^\alpha$ , with the exponent  $\alpha$  fitted in the insets depending on the specific circuit depth  $d_{\text{target}}$ . Since our algorithm does not require scalability with increasing  $d_{\text{target}}$

(which would be impossible), a small exponent around 2 for the target depth involved here is sufficient to demonstrate the efficiency and scalability of our algorithm for larger system sizes.

Next, we consider the scaling of quantum resources when accounting for circuit noise. The overall fidelity  $F_{\text{all}}$  and the optimal depth  $d_{\text{max}}$  for the state at  $d_{\text{target}} = 40$  and the unitary at  $d_{\text{target}} = 15$  are depicted in Fig. 3(c) and 3(f), respectively. The convergence of  $d_{\text{max}}$  with increasing system size  $N$  demonstrates that only a constant depth (and thus a linear dependence  $O(N)$  for the number of gates) is required to achieve the highest overall fidelity. This behavior is related to previous numerical studies, which show that a fixed error rate will lead to decoherence of the entire system after a constant circuit depth, regardless of the system size [30, 31].

### Real experiments on IBM quantum devices

We present experimental results of executing optimized circuits on IBM superconducting quantum computers 'ibm\_brisbane' to simulate the time evolution of the critical Ising model with  $N = 12$ ,  $\tau = 0.1$ , and  $t = 20$ . The hardware details are depicted in Fig. 4(a), where we use qubits 0 ~ 11 for our experiments. The target circuit is divided into  $m = 6$  parts, with  $d_{\text{target}}^{[1]} = 100$ ,  $d_{\text{target}}^{[j]} = 20$  for  $j = 2, \dots, 6$ , and  $d_{\text{optim}}^{[j]} = 8$  for  $j = 1, \dots, 6$ , corresponding to a total compression rate of  $\gamma = 3 \times 200/48 = 12.5$ . The results comparing the ideal target circuit, the experimental target circuit, the ideal optimized circuit, and the experimental optimized circuit are shown in Fig. 4(b), where the dynamics of a local observable  $\sigma_5^z \sigma_6^z$  are used to evaluate the performance. In the legend, "Target" and "Optimized" refer to the original time-evolution circuit and our optimized circuit, while "Ideal" and "Noisy" represent the results obtained from exact classical simulations and experiments on real quantum hardware. Error mitigation techniques including dynamical decoupling [32], Pauli twirling [33], twirled readout error extinction [34], and zero noise extrapolation [35] are integrated into the experiments.

The direct execution of the target circuit (blue circles) is hindered by decoherence, limiting it to depths of  $d_{\text{target}} = 50$ . Moreover, circuits exceeding depths  $d_{\text{target}} = 20$  cannot provide reliable results, highlighting the current limitations of quantum hardware in executing Trotter circuits for Hamiltonian evolution. In contrast, the implementation of our optimized circuit (red squares) enables effective simulation of the target dynamics up to  $d_{\text{target}} = 160$  (with  $d_{\text{optim}} = 32$ ), significantly extending the range of quantum simulation possible with NISQ quantum hardware by one order of magnitude. This result demonstrates the potential of approximate circuit compilation in overcoming the limitations of quantum hardware, especially in simulating more complex systems. We also extend our investigations to other observables, yielding similar results (not shown here). Furthermore, the comparison between ideal and experimental data for the optimized circuit in Fig. 4(b) reveals an important observation. The distance

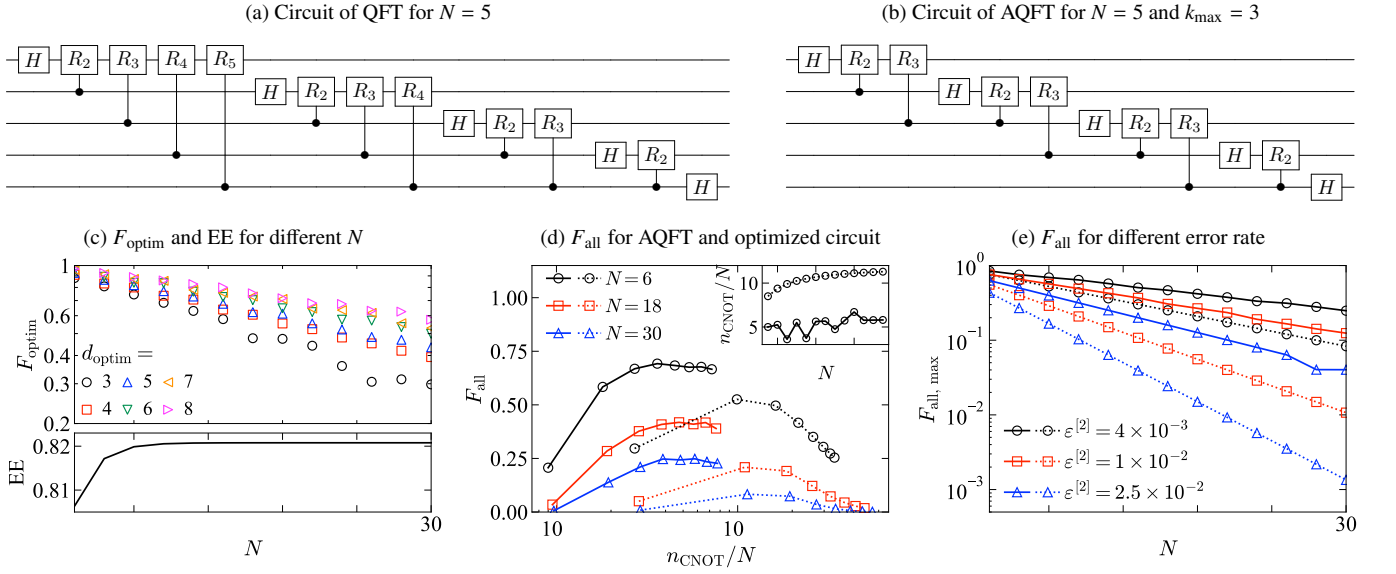


FIG. 5. Results for QFT without SWAP gates at the end. (a) Quantum circuit of QFT without the final SWAP gates. (b) Quantum circuit of AQFT for  $k_{\max} = 3$  without the final SWAP gates. (c) Optimization fidelity  $F_{\text{optim}}$  and EE for different  $N$  and  $d_{\text{optim}}$ . (d) Overall fidelity  $F_{\text{all}}$  of the optimized circuit (solid lines) and AQFT circuit (dotted lines) against the number of CNOT gates used. Insets compare the optimal  $n_{\text{CNOT}}/N$  for both circuits across different  $N$ . (e) Maximum of overall fidelity  $F_{\text{all,max}}$  of the optimized circuit (solid lines) and AQFT circuit (dotted lines) at different error rates.

between gray diamonds and the black curve is much smaller than the distance between gray diamonds and red squares, especially for large  $d_{\text{target}}$ . This suggests that noise effects in the optimized circuit still dominate over compilation errors, implying that further improvement in compression rate could be achieved. However, the trade-off between noise and compilation error is hardware-dependent, determined by the specific error rates of the quantum device. Therefore, an optimal depth should be carefully chosen for each specific task to maximize fidelity and fully leverage the potential of quantum computers.

### Quantum Fourier transformation

In the following, we focus on the QFT circuit, which plays a central role in many important and promising quantum algorithms [10]. The QFT circuit  $F_N$  can be decomposed as  $F_N = S_N Q_N$ , where  $Q_N$  is the core part that performs the Fourier transformation of the information encoded in the input state, as shown in Fig. 5(a).  $S_N$  is a sequence of SWAP gates that reverse the order of all qubits at the end of the circuit (not shown here). The circuit  $Q_N$  contains non-local control-rotation gates  $CR_k$ , where  $k$  is the interaction length and  $R_k$  represents the following rotation

$$R_k = \begin{bmatrix} 1 & 0 \\ 0 & e^{i\frac{2\pi}{k}} \end{bmatrix}. \quad (9)$$

It has been analytically proved that  $Q_N$  features a set of exponentially decaying Schmidt coefficients independent of the system size  $N$  [36]. This insight motivates us to investigate

a more compact version of this circuit, as the original configuration is quite sparse. Fig. 5(c) illustrates the optimization fidelity for the entire  $Q_N$  as  $N$  increases on a logarithmic scale, accompanied by the operator EE that clearly converges to a finite value as  $N$  grows. The exponential decay of  $F_{\text{optim}}$  with  $N$  is reasonable, since the circuit depth of  $Q_N$  scales quadratically with  $N$ , rather than being fixed.

Similar to the previous analysis, we also consider the impact of noise effects by assuming a fixed error rate  $\varepsilon^{[2]} = 4 \times 10^{-3}$  for the CNOT gates. The overall fidelity  $F_{\text{all}}$  and the corresponding number of CNOT gates  $n_{\text{CNOT}} = (N-1)d_{\text{optim}}$  (which quantifies the quantum resources required to execute the circuit) are depicted in Fig. 5(d) by solid lines. For comparison, we evaluate the performance of approximate QFT (AQFT) [37] shown in Fig. 5(b), where qubit rotations below a certain angle  $2\pi/k_{\max}$  are neglected, as illustrated in Fig. 5(d) by dotted lines. The number of CNOT gates used to compile the AQFT circuit is derived in Methods. The results indicate that our optimized circuit achieves higher accuracy than the AQFT circuit with the same amount of quantum resources. Meanwhile, the optimal  $n_{\text{CNOT}}$  to achieve maximal overall fidelity  $F_{\text{all}}$  compared in the inset of Fig. 5(d) demonstrate the reduction of quantum resources using our method. In addition, we compare the maximal overall fidelities  $F_{\text{all,max}}$  of both circuits for three typical values of error rates ( $\varepsilon^{[2]} = 4 \times 10^{-3}, 1 \times 10^{-2},$  and  $2.5 \times 10^{-2}$ ) in Fig. 5(e), representing different stages of NISQ quantum hardware before the realization of fault-tolerant systems. The results for the optimized circuit consistently show an advantage over the AQFT circuit across various noise levels. This advantage diminishes as the error rate decreases, suggesting reduced com-

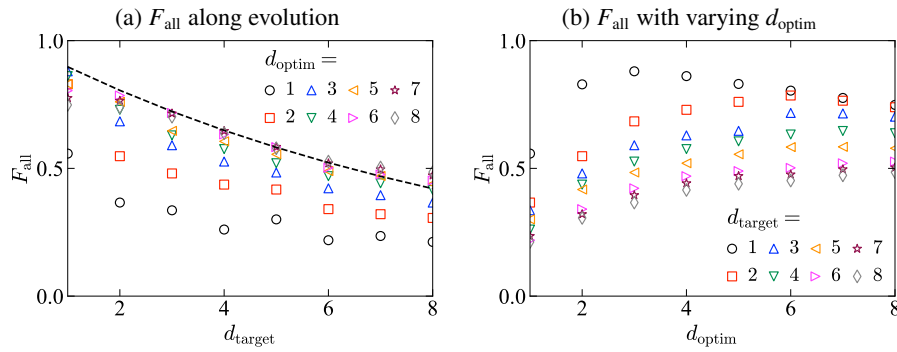


FIG. 6. Performance of circuit compilation for Haar random quantum circuits with  $N = 10$ . (a) Overall fidelity  $F_{\text{all}}$  with increasing target circuit depth  $d_{\text{target}}$  for different  $d_{\text{optim}}$ . The black dashed line represents the direct compilation of the target circuit. (b) Overall fidelity  $F_{\text{all}}$  with varying  $d_{\text{optim}}$  for different  $d_{\text{target}}$ .

pressibility for quantum devices with better performance.

### Haar Random quantum circuits

We evaluate the performance of our method by approximately compiling a Haar random quantum circuit and analyzing its characteristics. A Haar random circuit exhibits a brick-wall layout, where each two-qubit gate is drawn randomly and independently from the uniform distribution in the unitary group  $U(4 \times 4)$  [38]. Such circuits are characterized by ballistic growth of entanglement, which complicates their classical simulation using the tensor network methods and is often associated with quantum advantage [1]. The comparison in Fig. 6(a) for  $N = 10$  between direct compilation (black dashed line) and our approximate compilation method shows that little improvement can be achieved with our approach. Meanwhile, the optimal depth  $d_{\text{max}}$  identified in Fig. 6(b) suggests that the random circuit can be hardly compressed (with the compression rate  $\gamma = 1$  for  $d_{\text{target}} = 1, 2$ ). This limitation can be attributed to the fact that the target circuit quickly accumulates entanglement, which maximizes the entangling capacity of the two-qubit gates, leaving little room for further performance improvement.

### DISCUSSION

In this study, we propose an alternative procedure for executing quantum circuits by approximately compiling them into a brick-wall layout, where CNOT gates are the only two-qubit gates involved, as they are directly implementable on quantum computers. In general, our scheme can be integrated into various quantum computational tasks, enhancing overall accuracy and reducing experimental costs. However, as previously discussed, the effectiveness of our approach depends on how quickly entanglement accumulates in the target circuit, limiting its applicability to certain types of random circuits that exhibit ballistic entanglement growth. In the following, we discuss the implications of our results in different contexts.

An important observation is that, in the case of simulating the time evolution of a Hamiltonian, taking the Trotter step  $\tau$  to an infinitesimally small value ( $\tau \rightarrow 0$ ) would theoretically lead to an infinite compression rate ( $\gamma \rightarrow \infty$ ), which may seem ideal. However, this is not practically feasible, since the ultimate goal is to simulate the time evolution of quantum many-body models on quantum computers to achieve practical quantum advantage. In this case, for sufficiently small values of  $\tau$ , the approximate compilation error dominates, and the Trotter error becomes negligible. Therefore, pursuing an infinitely small  $\tau$  is unnecessary and may not yield substantial improvements. For quantum computers in the NISQ era, the key challenge is balancing the trade-off between compilation error and the noise effects inherent in current quantum hardware. Our scheme provides a pathway to help state-of-the-art NISQ devices transition from demonstrating quantum utility [15] to achieving a practical quantum advantage. In the long term, reducing compilation error with increased quantum resources will not be a major focus until fault-tolerant quantum computers become available.

Another promising direction is to apply our scheme to promote the implementation of important quantum algorithms such as Shor's factoring and Grover's searching algorithms. Our results for QFT indicate that a numerically optimized circuit can outperform an analytically constructed one in terms of approximately executing a quantum algorithm. Recent studies have explored the classical simulation of these algorithms using tensor network methods [36, 39, 40], demonstrating that at least certain parts of these algorithms exhibit low entanglement or slow entanglement accumulation. This implies that our scheme could be particularly effective in facilitating their fast and accurate execution. In summary, our approach has the potential to foster the realization of powerful quantum algorithms on currently available quantum devices before fully fault-tolerant, enabling solutions to practical problems in various fields.

## METHODS

### Fidelity for quantum states and unitaries

The fidelity between two normalized pure states is defined as

$$f(|\psi\rangle, |\phi\rangle) = |\langle\psi|\phi\rangle|^2. \quad (10)$$

In our study, this definition is generalized for two unitaries (operators) as

$$f(U_1, U_2) = \frac{1}{2^N} \left| \text{Tr}[U_1^\dagger U_2] \right|, \quad (11)$$

corresponding to the inner product in the operator space.

### Optimization of single-qubit gates

We employ the Riemann optimization [19] to determine the single qubit gates that minimize the loss functions in Eqs. (4) and (5). In each iteration step, we calculate the gradient  $\nabla_i$  for a gate (tensor)  $U_i$  using automatic differentiation. The gradient is projected onto the tangent space of the unitary manifold,

$$\nabla_i^p = \frac{1}{2} \left( U_i^\dagger \nabla_i - \nabla_i^\dagger U_i \right). \quad (12)$$

The gate is then updated according to

$$U_i \Rightarrow U_i e^{-\eta \nabla_i^p}, \quad (13)$$

where  $\eta$  is the current learning rate automatically adjusted by the Adam optimizer, whose hyperparameters take the conventional values  $\eta^0 = 1 \times 10^{-3}$ ,  $\beta_1 = 0.9$ ,  $\beta_2 = 0.999$ , and  $\epsilon = 10^{-8}$ .

### Circuit of QFT

QFT is the key ingredient of phase estimation, which constitutes many interesting quantum algorithms including order-finding and Shor factoring algorithms. For a system with  $N$  qubits, the QFT  $F_N$  on an orthonormal basis  $|0\rangle, \dots, |2^N - 1\rangle$  is defined as [10]

$$F_N |j\rangle = \frac{1}{2^{N/2}} \sum_{k=0}^{2^N-1} e^{2\pi i j k / 2^N} |k\rangle. \quad (14)$$

Alternatively, QFT can be expressed in the binary representation,

$$F_N |j_1, \dots, j_N\rangle = \frac{1}{2^{N/2}} \left( |0\rangle + e^{2\pi i 0 \cdot j_N} |1\rangle \right) \otimes \left( |0\rangle + e^{2\pi i 0 \cdot j_{N-1} j_N} |1\rangle \right) \otimes \dots \otimes \left( |0\rangle + e^{2\pi i 0 \cdot j_1 \dots j_N} |1\rangle \right), \quad (15)$$

where all decimals  $0.j_1 \dots j_m$  are in binary representation. The circuit shown in Fig. 5(a) implements the QFT, but with a reversing order of qubits, i.e.,

$$Q_N |j_1, \dots, j_N\rangle = \frac{1}{2^{N/2}} \left( |0\rangle + e^{2\pi i 0 \cdot j_1 \dots j_N} |1\rangle \right) \otimes \left( |0\rangle + e^{2\pi i 0 \cdot j_2 \dots j_N} |1\rangle \right) \otimes \dots \otimes \left( |0\rangle + e^{2\pi i 0 \cdot j_N} |1\rangle \right). \quad (16)$$

In the end, a set of SWAP gates  $S_N$  is required to complete the QFT algorithm.

### Compilation of AQFT circuit

When compiling the AQFT circuit on a real quantum device, the nonlocal gates  $CR_k$  will introduce additional costs determined by the involvement of SWAP gates. Fortunately, the rotation angle  $2\pi/k$  in  $R_k$  is inversely proportional to the interaction length  $k$ , suggesting a truncation of  $k_{\max}$  to control the quantum resources. This leads to the AQFT circuits shown in Fig. 5(b). Now we focus on the number of CNOT gates required to compile an AQFT circuit of  $N$  qubits with a fixed  $k_{\max} \leq N$ . The AQFT circuit naturally allows for a division into  $N$  rounds, where the first  $N - k_{\max} + 1$  rounds have the same structure, differing only by the translation of qubits. The remaining  $k_{\max} - 1$  rounds exhibit decreasing interaction lengths. Consider a round with maximum interaction length  $k$  and starting qubit  $j$ . To realize all nonlocal gates, we need to exchange the starting qubit with adjacent qubits to move it to site  $k + j - 2$ , followed by a backmovement. This results in a total number of  $k - 1$  (gates) +  $2(k - 2)$  (exchange) =  $3k - 5$  two-qubit gates. The interaction length and the corresponding number of two-qubit gates for each round are summarized in the following table.

Round No.	$k$	Two-qubit gate number
1	$k_{\max}$	$3k_{\max} - 5$
...	...	...
$N - k_{\max} + 1$	$k_{\max}$	$3k_{\max} - 5$
$N - k_{\max} + 2$	$k_{\max} - 1$	$3k_{\max} - 8$
...	...	...
$N - 1$	2	1
$N$	1	0

Summing over all rounds and considering that each two-qubit gate is compiled into three CNOT gates, we obtain the total number of CNOT gates as

$$n_{\text{CNOT}} = 3 \left[ (3k_{\max} - 5)(N - k_{\max} + 1) + \sum_{k=2}^{k_{\max}-1} (3k - 5) \right] \quad (17)$$

$$= 3 \left[ (3k_{\max} - 5)(N - \frac{k_{\max}}{2}) - (k_{\max} - 2) \right].$$



## DATA AVAILABILITY

The datasets generated and analyzed during the current study are available from the corresponding author upon reasonable request.

## CODE AVAILABILITY

The IBM Quantum device ‘ibm\_brisbane’ is accessible at <https://quantum-computing.ibm.com/>. The code for this study is available from the corresponding author upon reasonable request.

---

\* [shuoyang@tsinghua.edu.cn](mailto:shuoyang@tsinghua.edu.cn)

- [1] F. Arute *et al.*, Quantum supremacy using a programmable superconducting processor, *Nature* **574**, 505 (2019).
- [2] H.-S. Zhong *et al.*, Quantum computational advantage using photons, *Science* **370**, 1460 (2020).
- [3] A. Morvan *et al.*, Phase transitions in random circuit sampling, *Nature* **634**, 328 (2024).
- [4] J. Preskill, Quantum computing in the NISQ era and beyond, *Quantum* **2**, 79 (2018).
- [5] R. Orús, A practical introduction to tensor networks: Matrix product states and projected entangled pair states, *Ann. Phys.* **349**, 117 (2014).
- [6] J. I. Cirac, D. Pérez-García, N. Schuch, and F. Verstraete, Matrix product states and projected entangled pair states: Concepts, symmetries, theorems, *Rev. Mod. Phys.* **93**, 045003 (2021).
- [7] F. Pan and P. Zhang, Simulation of quantum circuits using the big-batch tensor network method, *Phys. Rev. Lett.* **128**, 030501 (2022).
- [8] F. Pan, K. Chen, and P. Zhang, Solving the sampling problem of the sycamore quantum circuits, *Phys. Rev. Lett.* **129**, 090502 (2022).
- [9] A. J. Daley *et al.*, Practical quantum advantage in quantum simulation, *Nature* **607**, 667 (2022).
- [10] M. A. Nielsen and I. L. Chuang, *Quantum Computation and Quantum Information* (Cambridge University Press, 2009).
- [11] S. Endo, Z. Cai, S. C. Benjamin, and X. Yuan, Hybrid quantum-classical algorithms and quantum error mitigation, *J. Phys. Soc. Jpn.* **90**, 032001 (2021).
- [12] M. Cerezo, A. Arrasmith, R. Babbush, S. C. Benjamin, S. Endo, K. Fujii, J. R. McClean, K. Mitarai, X. Yuan, L. Cincio, and P. J. Coles, Variational quantum algorithms, *Nat. Rev. Phys.* **3**, 625 (2021).
- [13] M. Cerezo, M. Larocca, D. García-Martín, N. L. Diaz, P. Braccia, E. Fontana, M. S. Rudolph, P. Bernejo, A. Ijaz, S. Thanasilp, E. R. Anschuetz, and Z. Holmes, Does provable absence of barren plateaus imply classical simulability? or, why we need to rethink variational quantum computing (2024), [arXiv:2312.09121](https://arxiv.org/abs/2312.09121).
- [14] M. Larocca, S. Thanasilp, S. Wang, K. Sharma, J. Biamente, P. J. Coles, L. Cincio, J. R. McClean, Z. Holmes, and M. Cerezo, A review of barren plateaus in variational quantum computing (2024), [arXiv:2405.00781](https://arxiv.org/abs/2405.00781).
- [15] Y. Kim, A. Eddins, S. Anand, K. X. Wei, E. van den Berg, S. Rosenblatt, H. Nayfeh, Y. Wu, M. Zaletel, K. Temme, and A. Kandala, Evidence for the utility of quantum computing before fault tolerance, *Nature* **618**, 500 (2023).
- [16] Y. Guo and S. Yang, Noise effects on purity and quantum entanglement in terms of physical implementability, *npj Quantum Inform.* **9**, 11 (2023).
- [17] I. A. Luchnikov, A. Ryzhov, S. N. Filippov, and H. Ouerdane, QGOpt: Riemannian optimization for quantum technologies, *SciPost Phys.* **10**, 079 (2021).
- [18] J. Gibbs and L. Cincio, Deep circuit compression for quantum dynamics via tensor networks (2024), [arXiv:2409.16361](https://arxiv.org/abs/2409.16361).
- [19] D. Rogerson and A. Roy, Quantum circuit optimization using differentiable programming of tensor network states (2024), [arXiv:2408.12583](https://arxiv.org/abs/2408.12583).
- [20] G. Vidal and C. M. Dawson, Universal quantum circuit for two-qubit transformations with three controlled-not gates, *Physical Review A* **69**, 010301 (2004).
- [21] M. Hauru, M. V. Damme, and J. Haegeman, Riemannian optimization of isometric tensor networks, *SciPost Phys.* **10**, 040 (2021).
- [22] R. Wiersema and N. Killoran, Optimizing quantum circuits with riemannian gradient flow, *Phys. Rev. A* **107**, 062421 (2023).
- [23] D. E. Rumelhart, G. E. Hinton, and R. J. Williams, Learning representations by back-propagating errors, *Nature* **323**, 533 (1986).
- [24] A. Novikov, M. Rakhuba, and I. Oseledets, Automatic differentiation for riemannian optimization on low-rank matrix and tensor-train manifolds (2021), [arXiv:2103.14974](https://arxiv.org/abs/2103.14974).
- [25] D. P. Kingma and J. Ba, Adam: A method for stochastic optimization (2017), [arXiv:1412.6980](https://arxiv.org/abs/1412.6980).
- [26] G. Bécigneul and O.-E. Ganea, Riemannian adaptive optimization methods (2019), [arXiv:1810.00760](https://arxiv.org/abs/1810.00760).
- [27] B. Brantner, Generalizing adam to manifolds for efficiently training transformers (2024), [arXiv:2305.16901](https://arxiv.org/abs/2305.16901).
- [28] A. Nahum, J. Ruhman, S. Vijay, and J. Haah, Quantum entanglement growth under random unitary dynamics, *Phys. Rev. X* **7**, 031016 (2017).
- [29] R. Acharya *et al.*, Quantum error correction below the surface code threshold, *Nature* **10.1038/s41586-024-08449-y** (2024).
- [30] K. Noh, L. Jiang, and B. Fefferman, Efficient classical simulation of noisy random quantum circuits in one dimension, *Quantum* **4**, 318 (2020).
- [31] Y. Guo and S. Yang, Locally purified density operators for noisy quantum circuits, *Chin. Phys. Lett.* **41**, 120302 (2024).
- [32] L. Viola and S. Lloyd, Dynamical suppression of decoherence in two-state quantum systems, *Phys. Rev. A* **58**, 2733 (1998).
- [33] J. J. Wallman and J. Emerson, Noise tailoring for scalable quantum computation via randomized compiling, *Phys. Rev. A* **94**, 052325 (2016).
- [34] E. van den Berg, Z. K. Mineev, and K. Temme, Model-free readout-error mitigation for quantum expectation values, *Phys. Rev. A* **105**, 032620 (2022).
- [35] K. Temme, S. Bravyi, and J. M. Gambetta, Error mitigation for short-depth quantum circuits, *Phys. Rev. Lett.* **119**, 180509 (2017).
- [36] J. Chen, E. Stoudenmire, and S. R. White, Quantum fourier transform has small entanglement, *PRX Quantum* **4**, 040318 (2023).
- [37] A. Barenco, A. Ekert, K.-A. Suominen, and P. Törmä, Approximate quantum fourier transform and decoherence, *Phys. Rev. A* **54**, 139 (1996).

- [38] M. P. Fisher, V. Khemani, A. Nahum, and S. Vijay, Random quantum circuits, *Annu. Rev. Condens. Matter Phys.* **14**, 335 (2023).
- [39] M. Niedermeier, J. L. Lado, and C. Flindt, Simulating the quantum fourier transform, grover's algorithm, and the quantum counting algorithm with limited entanglement using tensor networks, *Phys. Rev. Res.* **6**, 033325 (2024).
- [40] E. M. Stoudenmire and X. Waintal, Opening the black box inside grover's algorithm, *Phys. Rev. X* **14**, 041029 (2024).

## ACKNOWLEDGEMENTS

This work is supported by the National Natural Science Foundation of China (NSFC) (Grant No. 12475022, No. 12174214, and No. 92065205) and the Innovation Program for Quantum Science and Technology (Grant No. 2021ZD0302100).